SUPPORTING INFORMATION

Ultrasensitive optical imaging with lanthanide lumiphores

Ukrae Cho[1], Daniel P. Riordan[2,4], Paulina Ciepla[1], Kiranmai S. Kocherlakota[1,5], James K. Chen[1,3,*], and Pehr B. Harbury[2,*]

[1]Department of Chemical and Systems Biology; [2]Department of Biochemistry; [3]Department of Developmental Biology, Stanford University School of Medicine, Stanford, California 94305, USA

[4]Present address: 10X Genomics, Pleasanton, California 94566, USA
[5]Present address: Chan-Zuckerberg Biohub and Department of Bioengineering, Stanford University School of Engineering, Stanford, California 94305, USA

*Correspondence should be addressed to J.K.C. (jameschen@stanford.edu) or P.B.H. (harbury@stanford.edu)

TABLE OF CONTENTS

Supplementary Table 1. Comparison of LED and Q-switched laser light sources

Specification	LED (Prizmatix, Mic-LED-365)	QSL*** (Spectra-Physics, Explorer One 355-300)
Pulse width	Variable, but typically 1 ms	< 15 ns (FWHM)
Power at output	250 mW*	Maximum of 300 mW (50 kHz)*
Beam diameter at output*	22 mm	0.170 ± 0.025 mm
Beam divergence (full angle)*	40 mrad	< 3.0 ± 0.5 mrad
Distance from the output to the stage	30 cm	130 cm
Beam diameter at the stage	4 mm	4 mm
Power at the objective back aperture (during pulse-on time)	120 mW**	N/A
Power at the stage (during pulse)	50 mW (6.3x UVI objective)	33 W (1-μJ pulse)
Power at the stage (time-averaged)	12 mW (1-ms pulses at 240 Hz)	7.5 mW (1-μJ pulses at 15 kHz)
Irradiance at stage (time-averaged)	95 mW/cm^2 (1-ms pulses at 240 Hz)	60 mW/cm^2 (1-μJ pulses at 15 kHz)

* Values provided by the manufacturer.
** The diffuser positioned between the light source and microscope main body was removed to maximize light transmittance.
*** Light transmission efficiency between QSL and microscope stage was determined to be ~50%.

Supplementary Table 2. Acquisition configurations for time-resolved luminescence imaging. A 360/40-nm band-pass excitation filter was used for all time-resolved imaging studies.

Figure	Light source	QSL pulse energy (μJ)	Objective	LRET acceptor	Emission filter (nm)	Cycle period (μs)	Excitation (μs)	Delay (μs)	Collection (μs)	Excitation frequency (Hz)	Total pulse number	Total imaging time (sec)
2a	LED	N.A.	5x	– Atto 610	> 575	3,333	10	Variable	500	300	2,000	6.7
	LED	N.A.	5x	+ Atto 610	> 575	3,333	10	Variable	500	300	1,000	3.3
2c	LED	N.A.	5x	– Atto 610	> 575	2,222	1	1	2,000	450	1,500	3.3
	LED	N.A.	5x	+ Atto 610	> 575	56	1	1	50	18,000	60,000	3.3
2d	LED	N.A.	6.3x	– Atto 610	> 575	6,667	Variable	2	2,030	150	250	1.7
	LED	N.A.	6.3x	+ Atto 610	> 575	6,667	Variable	2	74	150	250	1.7
3a	LED	N.A.	5x/6.3x	N.A.	> 575/615/25	3,333	250	Variable	2,000	300	1,000	3.3
4b	LED	N.A.	Variable	N.A.	> 575	2,222	25	10	2,000	450	375	0.83
	QSL	1.6	Variable	N.A.	> 575	2,222	1	10	2,000	450	375	0.83
4c	QSL	14.6	10x	N.A.	> 575	2,222	1	1	2,000	450	750	1.7
5a	LED	N.A.	6.3x	N.A.	> 575	6,667	Variable	10	2,000	150	25	0.17
	QSL	Variable	6.3x	N.A.	> 575	6,667	1	10	2,000	150	25	0.17
6a	QSL	15.0	10x	– Atto 610	> 575	3,333	1	1	2,853	300	1,000	3.3
	QSL	1.0	10x	+ Atto 610	> 575/655/40	67	1	1	63	15,000	50,000	3.3
6b	QSL	0.5	6.3x	+/– Atto Rho14	> 575/655/40	67	1	1	60	15,000	50,000	3.3
S3	LED	N.A.	5x	N.A.	> 575	1,333	200	300	800	750	5,000	6.7
S9c	LED	N.A.	6.3x	– Atto 610	> 575	4,167	1,000	1	2,853	240	8	0.033

	QSL	20.0	6.3x	+ Atto 610	> 575	46	1	1	42	21,750	725	0.033
S10a	QSL	1.3	10x	+ Atto 610	> 575	3,333	1	Variable	2,000	300	100	0.3
S11	LED	N.A.	6.3x	N.A.	> 575	4,167	100	1	Variable	240	400	1.7

Supplementary Table 3. Acquisition configurations for homogeneous solution assays.

Figure	Eu^{3+} complex	Interacting molecules	Excitation (nm)	Emission (nm)	Delay (μs)	Collection (μs)	Excitation frequency (Hz)	Total pulse number
S2b	Eu^{3+}/ATBTA Eu^{3+}/DTPA-cs124-CF_3	dNTP	330-350	614	20	100	100	10
S2c	Eu^{3+}/ATBTA Eu^{3+}/DTPA-cs124-CF_3	Ascorbate	330-350	604-640	50	450	100	20
1c	Eu^{3+}/ATBTA	Sulfo-Cy3 Sulfo-Cy5 Atto 610	330-350	550-750	Variable	100	100	10
1d	Eu^{3+}/ATBTA	Atto 610	330-350	550-750	30	1,000	100	20

Supplementary Table 4. Secondary antibodies for whole-mount immunostaining of zebrafish embryos

Figure	Antibody	Label	Source	Product Number	Concentration
4c	Goat anti-mouse IgG (H+L)	Alexa Fluor 405	Thermo Fisher Scientific	A-31553	1 μg/mL
		Alexa Fluor 488		A-11001	
		Alexa Fluor 594		A-11032	
		Eu^{3+}/DTBTA	Jackson ImmunoResearch	115-005-146	
6a	Goat anti-mouse IgG (H+L)	Alexa Fluor 594	Thermo Fisher Scientific	31160	Variable
		Eu^{3+}/DTBTA			

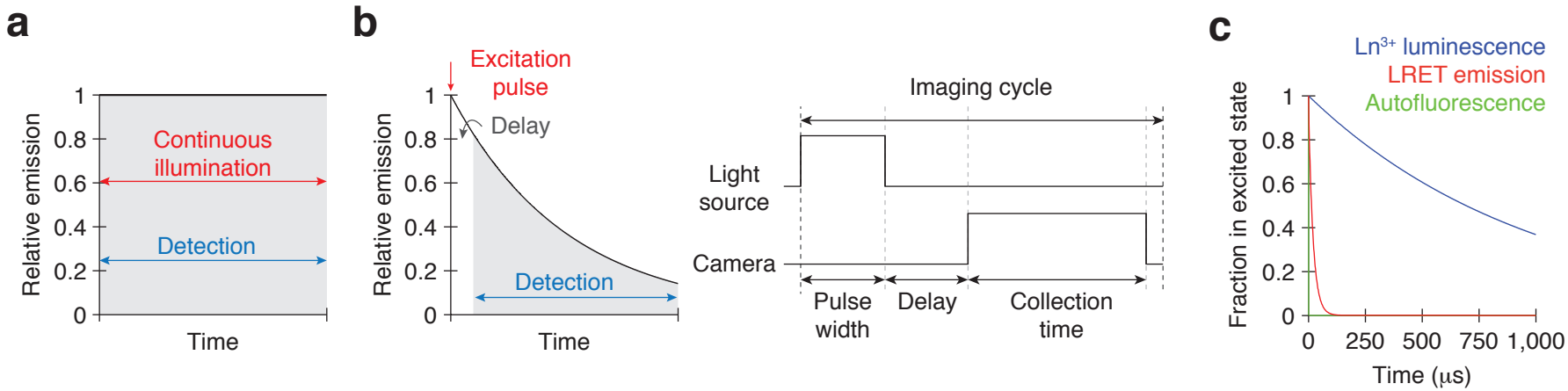

Supplementary Figure 1. Time-resolved lanthanide detection. Excitation and detection regimens for (a) steady-state fluorescence and (b) time-resolved luminescence microscopy. (c) Theoretical decay curves of Eu^{3+} (blue; τ = 1,000 μs), LRET (red; τ = 20 μs), and fluorescence (green; τ = 0.01 μs) emissions.

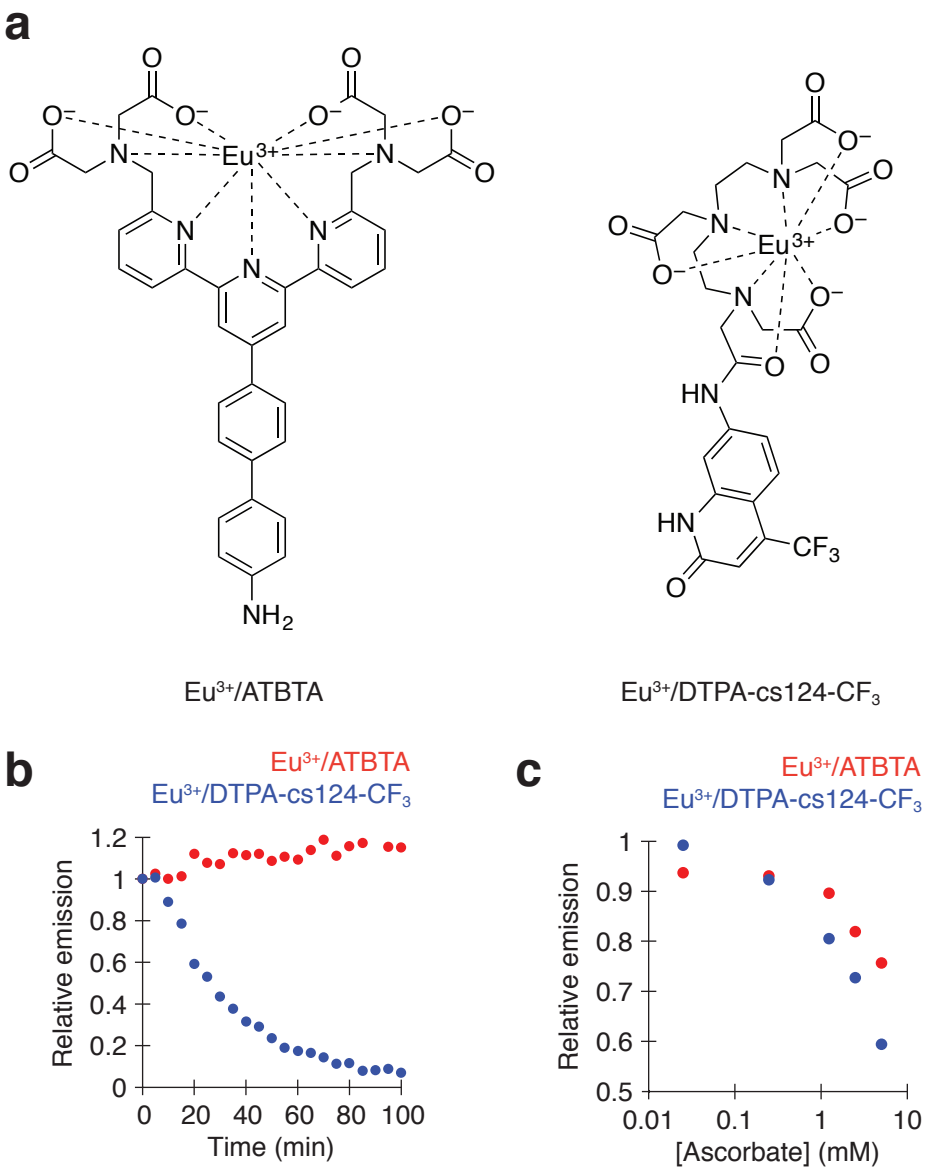

Supplementary Figure 2. Chemical properties of selected Eu^{3+} complexes. (a) Chemical structures of Eu^{3+}/ATBTA and Eu^{3+}/DTPA-cs124-CF_3. (b) Differential resistance of Eu^{3+}/ATBTA and Eu^{3+}/DTPA-cs124-CF_3 to 2 mM dNTPs. Each lanthanide complex was tested at a 0.5-μM concentration. (c) Concentration-dependent quenching of Eu^{3+}/ATBTA and Eu^{3+}/DTPA-cs124-CF_3 luminescence by ascorbate (0.5-μM solutions for each Eu^{3+} complex).

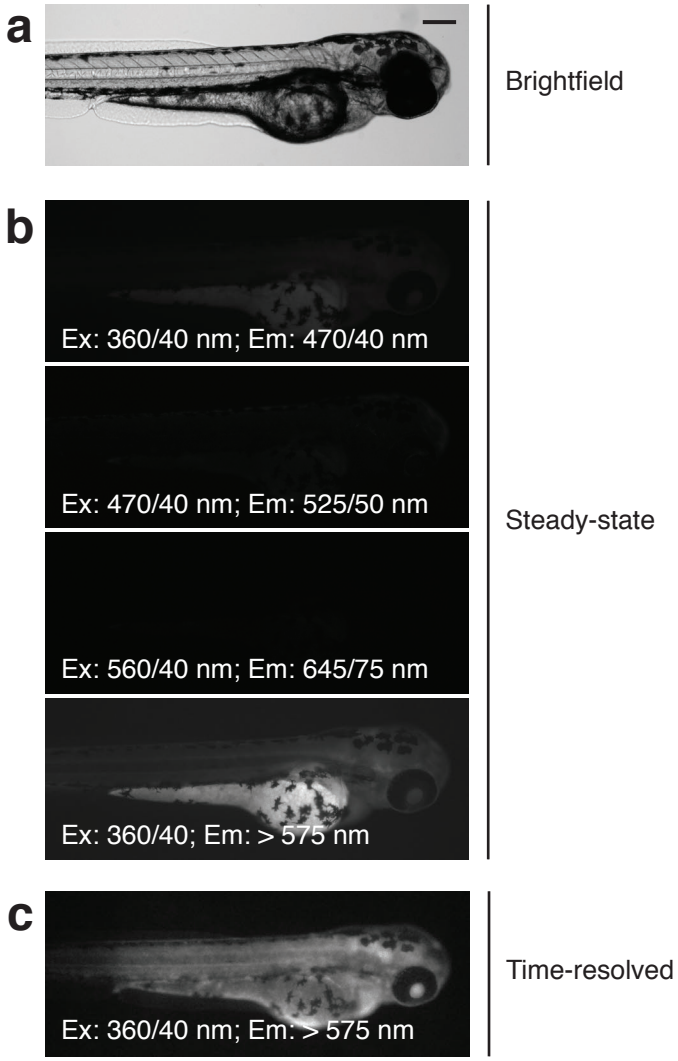

Supplementary Figure 3. Steady-state and time-resolved luminescence imaging of lanthanide complexes in zebrafish embryos. Zebrafish zygotes were injected with a Eu^{3+}/ATBTA-labeled MO (60 fmol/embryo) and then imaged at 3-dpf by brightfield (a), steady-state luminescence (b), or time-resolved luminescence (c) microscopy. All steady-state fluorescence micrographs were acquired using the designated filtersets and a 250-ms acquisition time. Time-resolved microscopy was conducted with the indicated filterset and imaging cycles composed of a 200-μs excitation pulse, 300-μs delay, and 800-μs emission acquisition period. Scale bar: 200 μm.

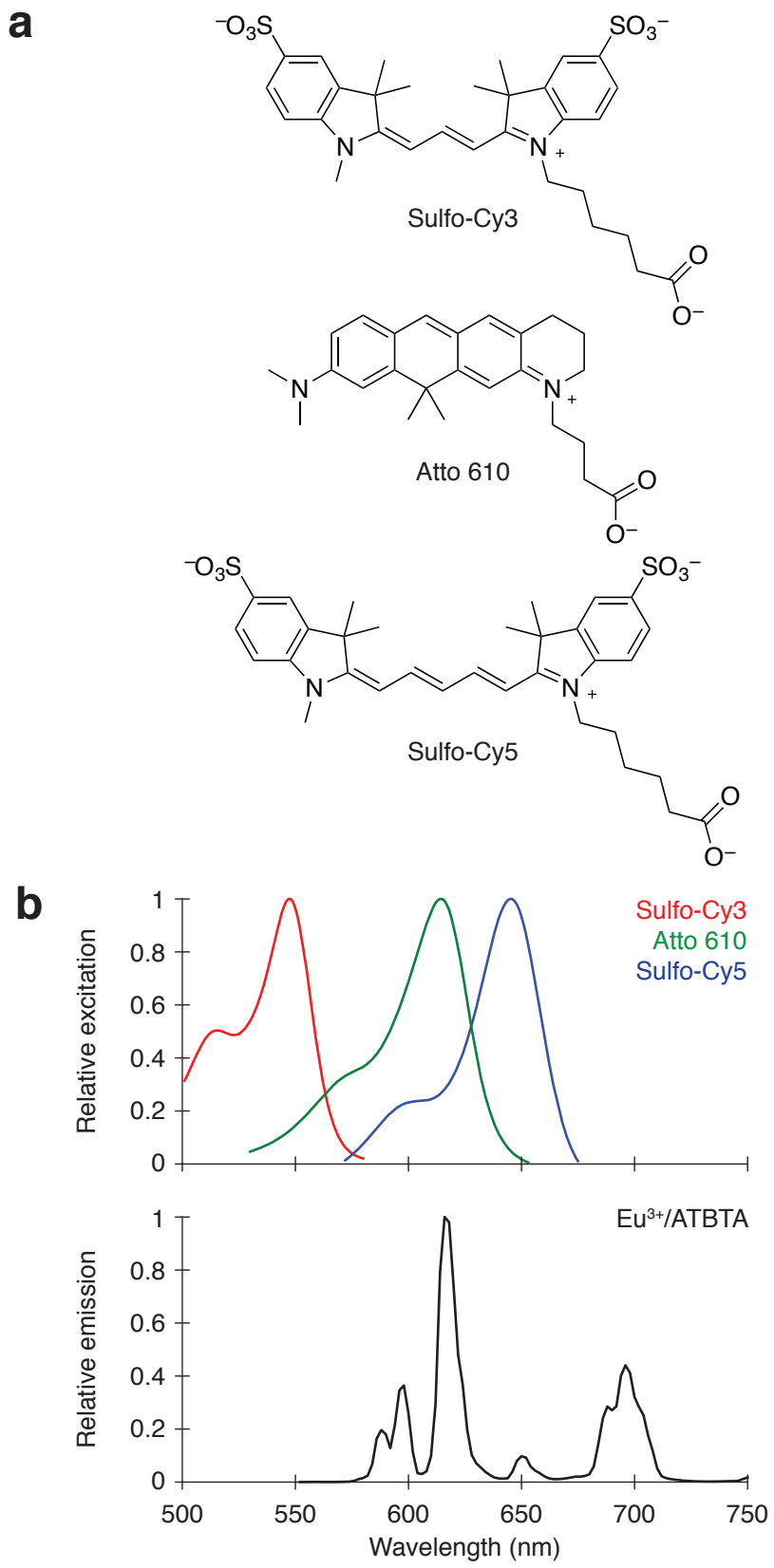

Supplementary Figure 4. Comparison of excitation spectra of LRET acceptors and the Eu^{3+}/ATBTA emission spectrum. (a) Chemical structures of Sulfo-Cy3, Atto 610, and Sulfo-Cy5. (b) The LRET acceptors reduce Eu^{3+}/ATBTA luminescence lifetime with efficiencies that correlate with the overlap between their excitation spectra and the Eu^{3+}/ATBTA emission spectrum.

a

$$A \text{ (ground state)} \underset{k_{em}}{\overset{k_{ex}}{\rightleftharpoons}} B \text{ (excited state)}$$

$$X(t) = \frac{k_{ex}}{k_{ex} + k_{em}} (1 - e^{-(k_{ex}+k_{em})t}) \quad \text{(initial condition: } X(0) = 0)$$

b

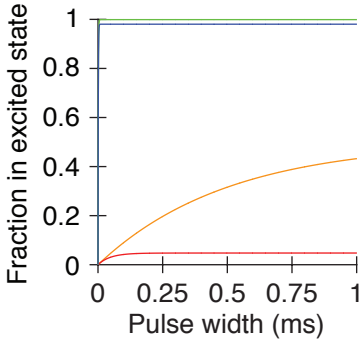

	k_{ex} (s^{-1})	τ_{ex} (μs)	k_{em} (s^{-1})	τ_{em} (μs)
—	10^6	1	10^3	1,000
—	10^6	1	20×10^3	50
—	10^3	1,000	10^3	1,000
—	10^3	1,000	20×10^3	50

Supplementary Figure 5. Kinetic analysis of lanthanide excitation. (a) Exponential equation describing the relationship between lanthanide excited-state fraction (X(t)), excitation and emission rates (k_{ex} and k_{em}), and illumination pulse duration (t). (b) Theoretical lanthanide excitation curves for different combinations of excitation and emission rates.

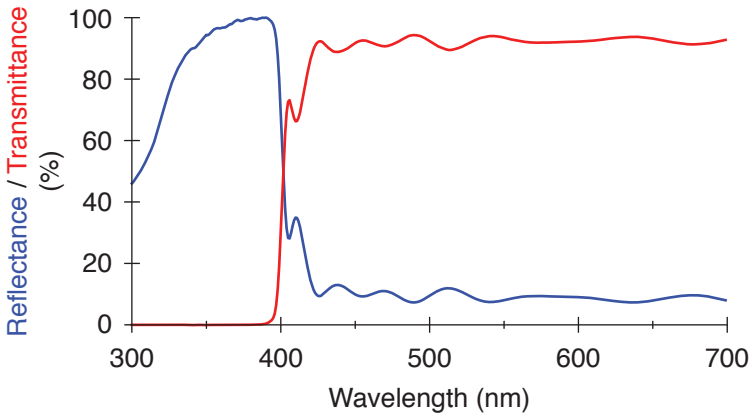

Supplementary Figure 6. Reflectance and transmittance curves of the TiO_2-coated coverglass. The UV-rejecting coverglass used for QSL trans-illumination includes include a TiO_2 coating and an overlying SiO_2 layer for chemical stability. The majority of 355-nm QSL light is reflected by the TiO_2 coating, and the rest is absorbed. A 0° angle of incidence was used to measure the reflectance and transmittance curves, and the TiO_2/SiO_2 layer thickness is negligible compared to that of the coverglass (0.2-mm thick fused silica).

a

	Energy (μJ)	k_{ex} (s^{-1})	τ_{ex} (ns)	k_{em} (s^{-1})	τ_{em} (μs)
QSL	25.7	29.3×10^6	34.2	1.05×10^3 (– LRET) or 27.8×10^3 (+ LRET)	951 (– LRET) or 36.0 (+ LRET)
	20.2	24.3×10^6	41.2		
	15.6	19.8×10^6	50.6		
	10.3	14.3×10^6	70.1		
	5.4	6.42×10^6	156		
	2.3	2.02×10^6	494		
LED		357	2.80×10^6		

b

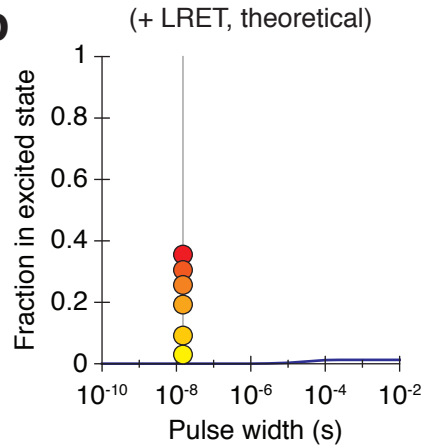

Supplementary Figure 7. QSL enables efficient excitation of lanthanide probes both in the presence and absence of LRET. (a) QSL k_{ex} values calculated using the data acquired in Fig. 5a and the equation described in Supplementary Fig. 5. (b) Predicted LED- or QSL-induced excited-state levels in the presence of LRET (τ_{em} = 36.0 μs).

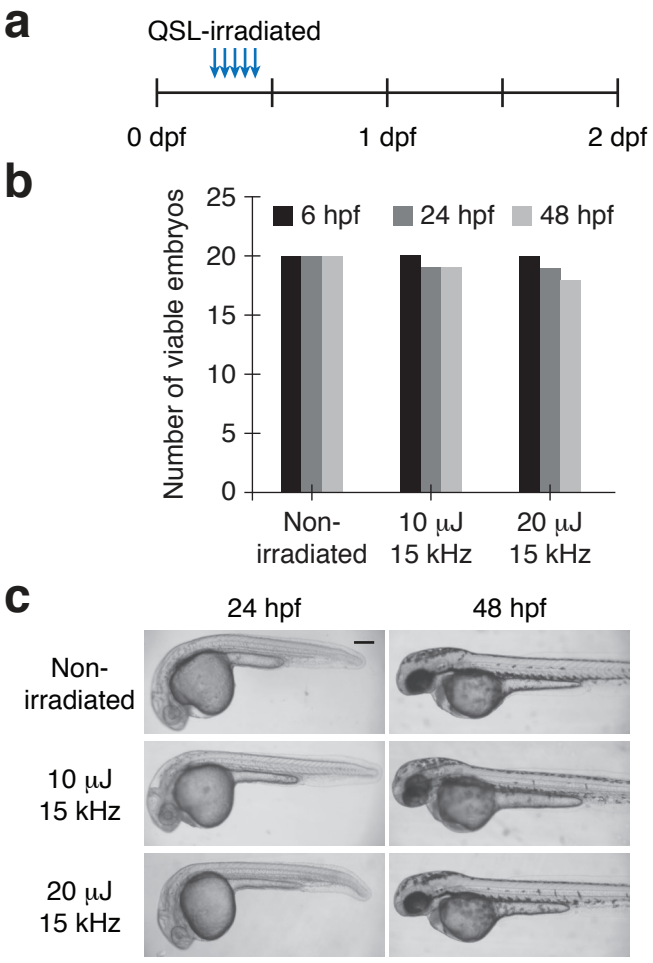

Supplementary Figure 8. QSL irradiation has minimal effects on zebrafish development. Zebrafish zygotes were irradiated with QSL every hour between the shield and bud stages (6-10 hpf; 5 irradiations in total) and subsequently analyzed at 24 and 48 hpf for evidence of developmental defects or toxicity. 10- or 20-μJ QSL pulses were given at 15 kHz over a 3.3-s period for each irradiation. 1-μJ QSL pulses with similar frequencies and total durations are typically employed for trLRET imaging. Scale bar: 200 μm.

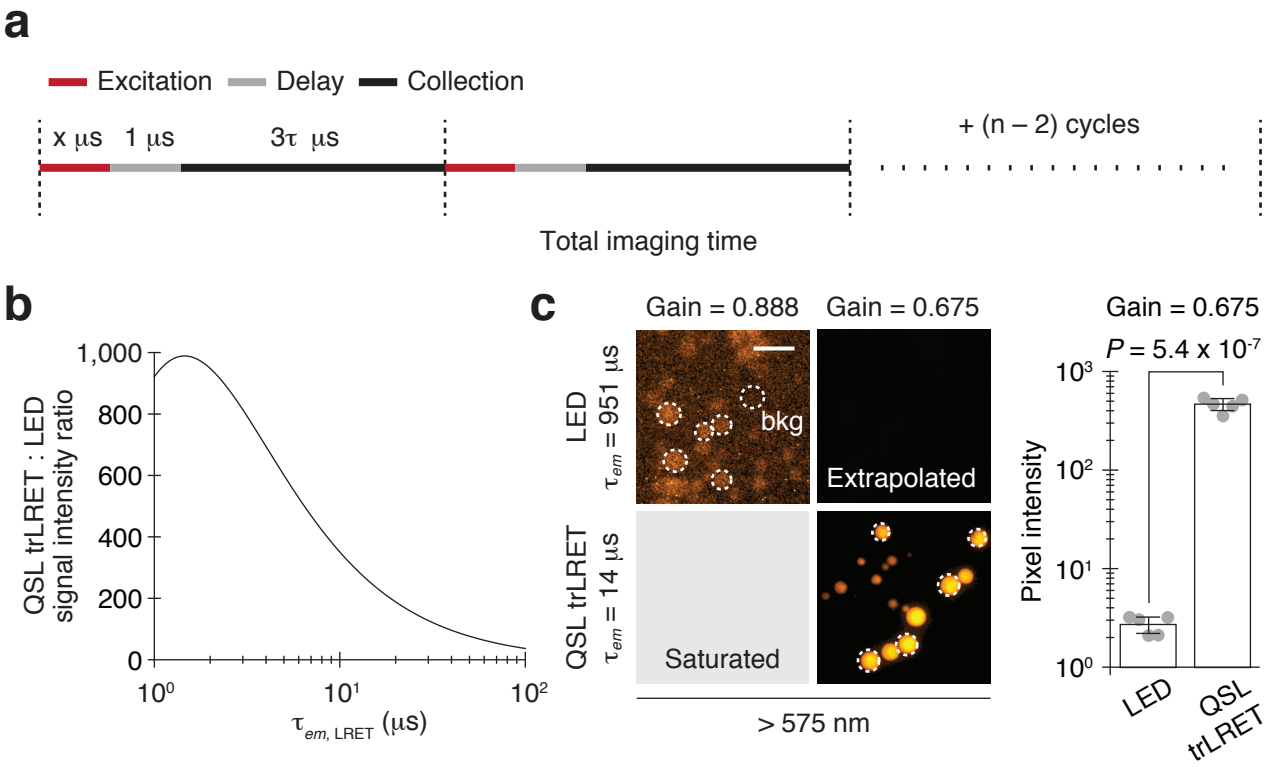

Supplementary Figure 9. Quantitative comparison of LED- and QSL trLRET-based time-resolved imaging. (a) Excitation, delay, and collection parameters used to compare LED epi-illumination and QSL trans-reflected illumination with LRET enhancement (see Supplementary Fig. 10 for further details). (b) Predicted QSL trLRET:LED signal intensity ratios for differing LRET-enhanced luminescence lifetimes ($\tau_{em,\ LRET}$) when LRET efficiencies are high (> 90%). (c) Eu^{3+}/ATBTA-functionalized beads imaged by time-resolved microscopy using the designated camera gain settings (0.675 or 0.888) and either LED epi-illumination or QSL trLRET. Total imaging times were identical for all conditions, and average signal intensities ± s.d. of selected beads (n = 5, dashed circles) are shown, adjusted for gain-dependent camera sensitivity as described in Supplementary Fig. 11. Scale bar: 200 μm.

a

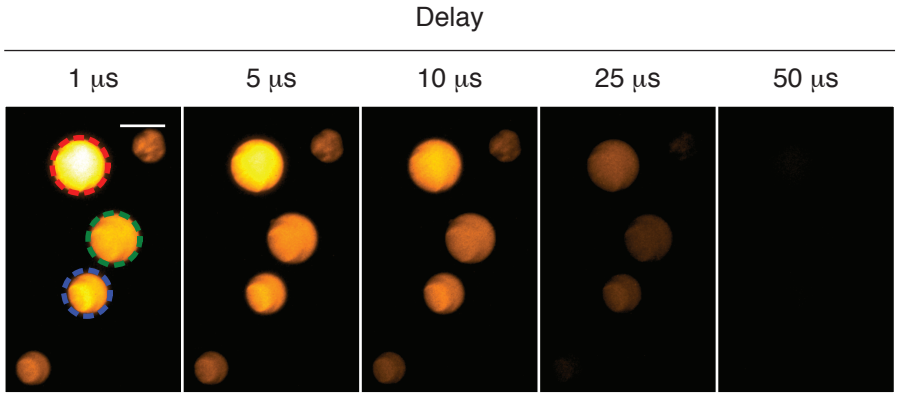

b

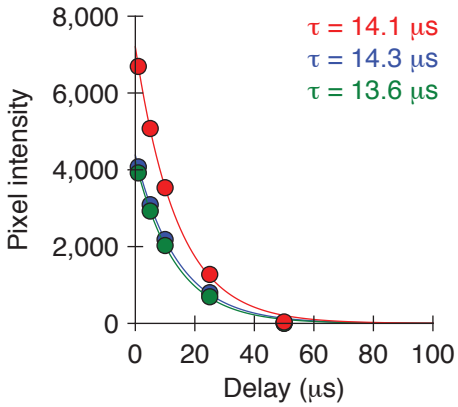

c

		LED	QSL trLRET
	Excitation	1,000 μs	1 μs
	Delay	1 μs	1 μs
	Collection (3τ)	3 × 951 μs	3 × $\tau_{em,\ LRET}$ μs
	Cycle period	4,167 μs	2 + 3$\tau_{em,\ LRET}$ μs
1	Cycle rate	240 Hz	10^6 / (2 + 3$\tau_{em,\ LRET}$) Hz
2	Quantum yield	0.38 (QY_{Eu})	E_{LRET} × $QY_{Atto\ 610}$
3	Fraction of probes excited	0.19 ($LED_{1\ ms}$)	0.31 ($QSL_{20.2\ \mu J}$)
4	Fraction decayed in 3τ μs	$\frac{\int_1^{1+3\tau} e^{-t/\tau}\,dt}{\int_0^{\infty} e^{-t/\tau}\,dt}$	
	Relative signal intensity	1 × 2 × 3 × 4	

Supplementary Figure 10. Quantitative modeling of LED- and QSL trLRET-based lanthanide imaging. (a) Time-resolved microscopy of Eu^{3+}/ATBTA-functionalized beads immersed in an aqueous solution of 30 μM Atto 610. The beads were pulse-illuminated with a QSL light source and then imaged after the designated delays. (b) Luminescence decay profiles of beads color-coded in (a). The data were fit to a first-order decay model to obtain the indicated average luminescence lifetimes, with R^2 values of 0.9989 (red, 0.9984 (blue), and 0.9989 (green). (c) Parameters used to estimate integrated Eu^{3+}/ATBTA signal intensities for LED epi-illumination versus QSL trLRET illumination. Scale bar: 100 μm.

a

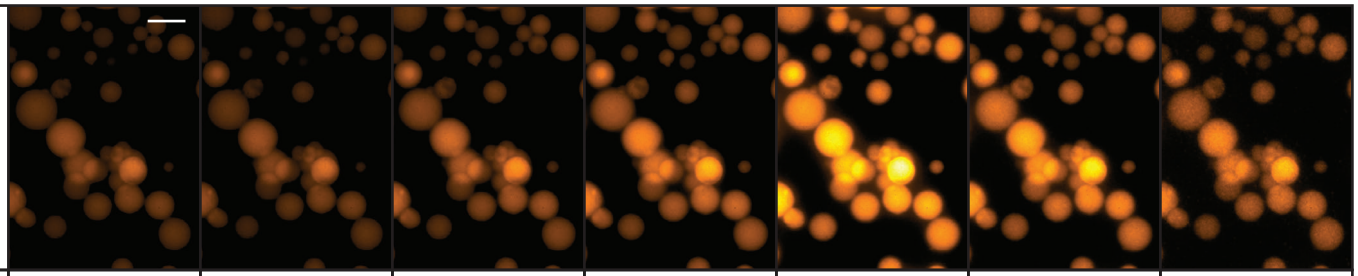

Camera gain	0.600	0.650	0.675	0.700	0.750	0.800	0.888
Collection (μs)	1,000	300	250	200	150	50	10
Fraction decayed	0.65	0.27	0.23	0.19	0.15	0.051	0.010
Mean intensity	1,593	1,609	2,315	3,066	6,066	4,326	3,350
Relative sensitivity	0.24	0.59	1	1.6	4.1	8.5	33

b

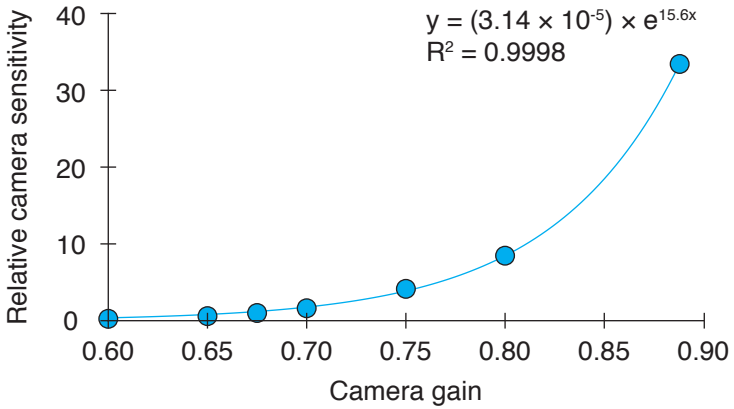

Supplementary Figure 11. Relative camera sensitivity at different gain values. (a) Time-resolved imaging of Eu^{3+}/ATBTA-functionalized beads using different camera gains and varying emission acquisition times to obtain pixel intensities within the linear dynamic range of the micrograph. All imaging protocols utilized a fixed delay of 1 μs. The mean pixel intensity for each image was then normalized with respect to the lanthanide excited-state decay during emission acquisition (fraction decayed) to obtain relative differences in camera sensitivity. Scale bar: 100 μm. (b) Graphical representation of the relationship between camera gain and sensitivity. The data points were fitted to an exponential curve.

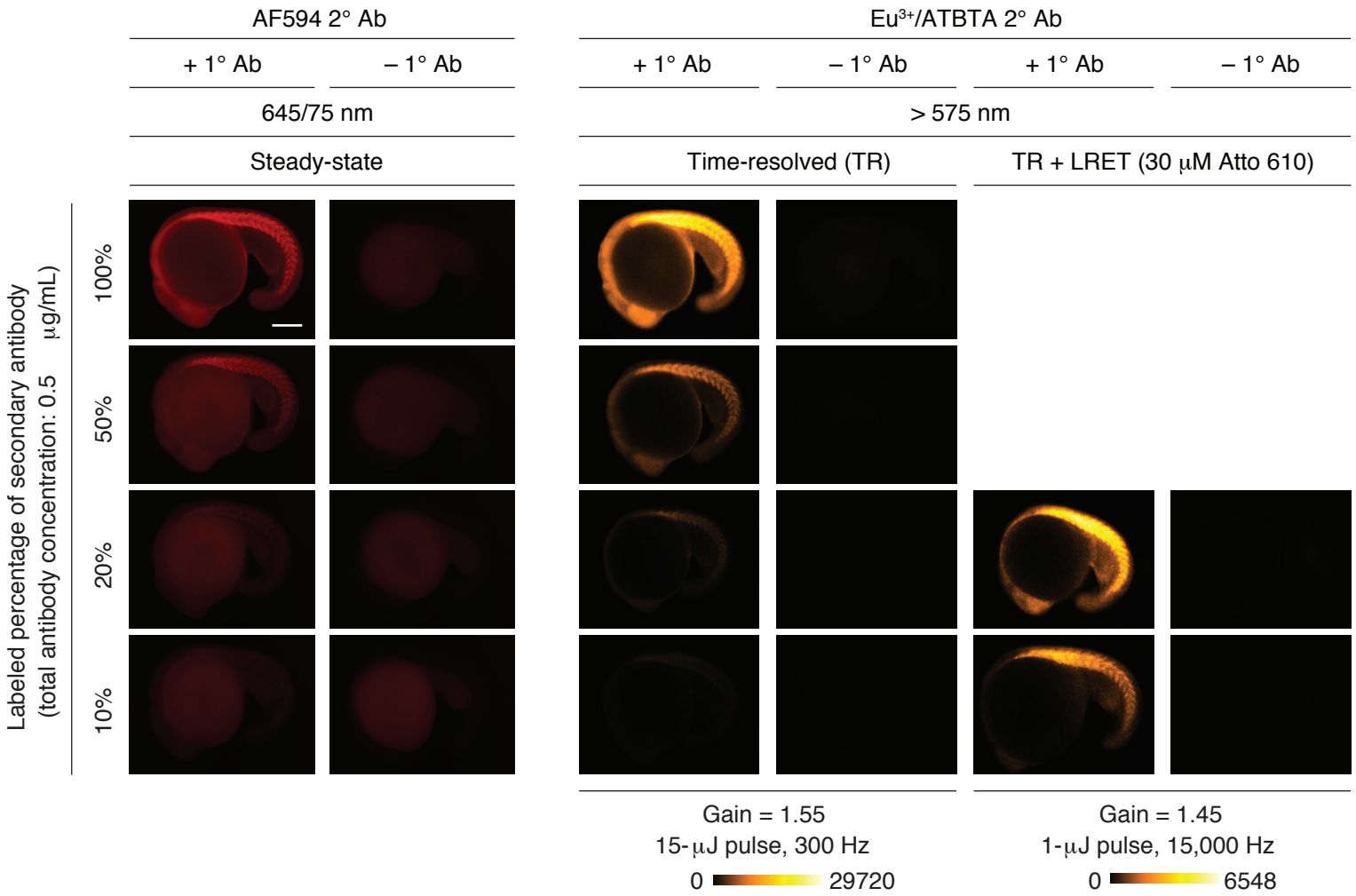

Supplementary Figure 12. Assessment of background signals in whole-mount lanthanide imaging. To determine the origin of non-somitic signals in zebrafish embryos stained with an anti-MYH1E antibody and labeled secondary antibodies (Fig. 6a), we stained the fixed embryos with either AF594- or Eu^{3+}/ATBTA-conjugated secondary antibody in the presence or absence of the anti MYH1E antibody. Yolk autofluorescence was detected by steady-state fluorescence imaging but suppressed by time-resolved luminescence imaging. Background signals from non-somitic animal cells were predominantly due to non-specific binding of the anti-MYH1E antibody and detected by both imaging modalities. Signals due to animal cell autofluorescence or non-specific binding of the labeled secondary antibodies were too low to reliably quantify in these experiments. Antibody concentrations, incubation times, and imaging configurations were identical to those used for the studies shown in Fig. 6a. Scale bar: 200 μm.

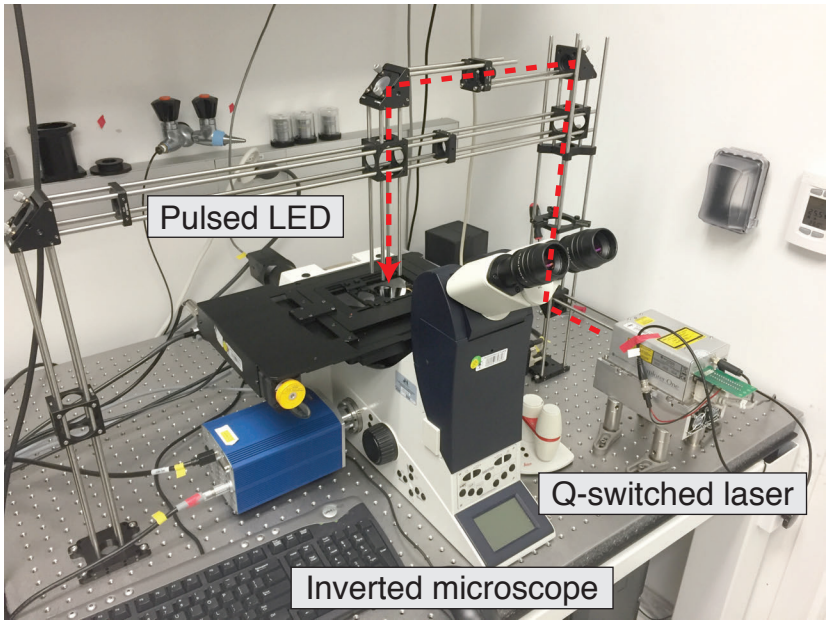

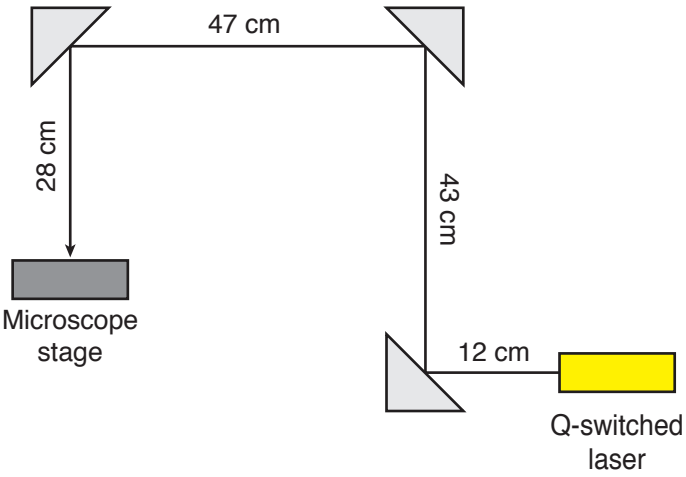

Supplementary Figure 13. QSL trLRET imaging instrumentation. A QSL light path was built around a Leica DMI6000B inverted microscope using the indicated optomechanical components for 30-mm and 60-mm cage systems, and the laser was fixed onto an optical table using pillar posts and clamping forks. All Components were obtained from Thorlabs. Steady-state fluorescence and time-resolved imaging cameras were installed at the left and right detector ports, respectively (right port hidden by the microscope body in the photo). A pulsed LED was connected to the built-in module for epi-illumination light sources. The camera and light sources were synchronized by a pulse generator (not shown), and the integrated system was controlled with Piper software (version 2.6.84).

Cage system components for QSL light path
- Ø6 mm cage rod (1"-, 2"-, and 12"- long; ER1, ER2, and ER12)
- 30 mm cage cube (C6W)
- 30 mm cage plate (CP06)
- 30 mm-to-60 mm cage plate adapter (LCP02)
- 60 mm cage plate (LH160C)
- Vertical mounting plate (CPVM)

Mirrors
- Ø1" UV-enhanced mirror (PF10-03-F01)
- Mirror mount (KCB1C)

QSL installation
- Ø1" pillar post (0.75"- and 2"-long; RS2P and RS075)
- Clamping fork (CF125C)

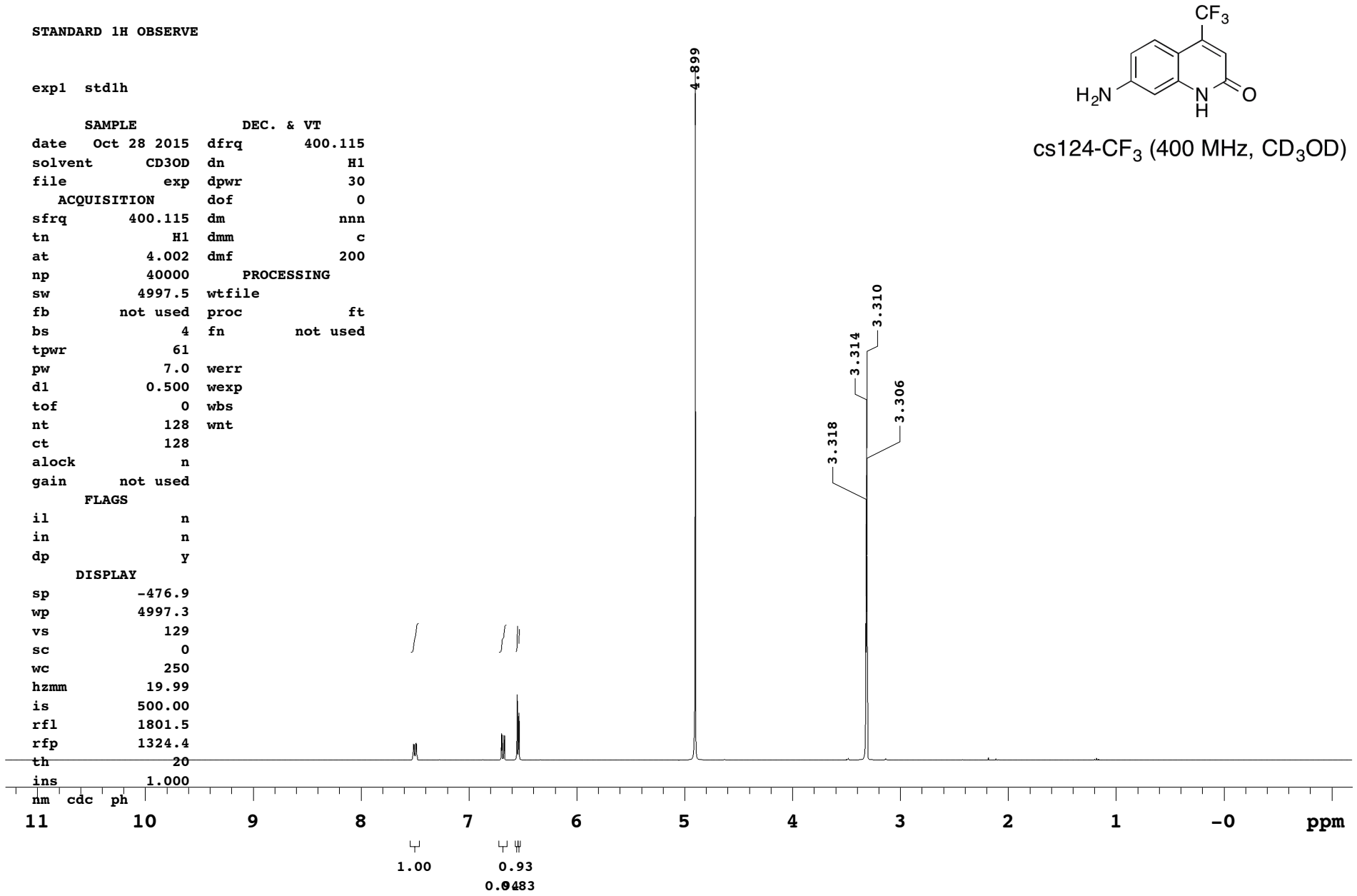

Supplementary Figure 14. ^{1}H NMR spectrum of cs124-CF_3.

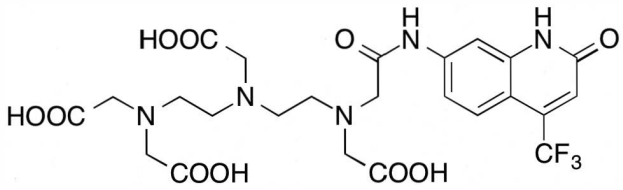

DTPA-cs124-CF_3 (400 MHz, CD_3OD)

Supplementary Figure 15. ^1H NMR spectrum of DTPA-cs124-CF_3.